Multidisciplinary Control Co-Design Optimization of Anguilliform-Swimming Soft Fluidic Robots

Abstract— **Anguilliform-swimming soft fluidic robots hold great promise for a range of underwater applications. However, because they leverage the complex dynamics of soft bodies interacting with fluids, it is challenging to use intuition to determine design parameters. Multidisciplinary design optimization offers a promising solution to this challenge by providing an automated and systematic method for leveraging computational models to find optimal design parameters. There have been design optimization studies in soft robotics, and there have been multidisciplinary design optimization studies in other fields, such as aircraft design, but the intersection of multidisciplinary dynamic modeling for design optimization of soft robots is relatively unexplored. This study investigates a method for multidisciplinary control co-design optimization of anguilliform-swimming soft robots, using physics-based models to optimize shape and control parameters. The modeling framework includes a geometry-centric approach for geometry modeling and parametrization, a three-dimensional finite element model for structural mechanics, and an unsteady panel method for fluid dynamics. The approach is tested by applying it to the optimization of a pre-existing eel-inspired soft robot. Model parameters are estimated based on existing experimental data, and two control co-design optimizations, with high-level and multilevel shape parametrizations, are performed to minimize energy cost. The optimized designs show a simulated energy cost reduction of 55% and 73% for the high-level and multilevel parametrizations, respectively, with an increase in swimming speed of 128%. The optimized actuator module is manufactured, and used to collect additional data for re-estimating the structural model parameters. The optimization is performed again with the updated model parameters, showing a simulated energy cost reduction of 45% and the prescribed 128% speed increase compared to the baseline design with optimized control and updated model parameters. These results demonstrate the potential of the proposed optimization approach to advance the performance of anguilliform-swimming soft fluidic robots.**

I. Introduction

Soft, anguilliform-swimming robots hold great promise for a range of aquatic applications. Due to their soft material and fish-like swimming motion, these robots can navigate underwater environments with minimal disturbance, making them ideal for delicate tasks such as exploring oceans [1] or marine ecosystems [2]. Anguilliform-swimming robots, which mimic the whole-body undulating motion seen in eels and oarfish, are of particular interest due to their energy efficiency [3]. Additionally, fluidic elastomer actuators offer a promising approach for powering these robots due to their ability to generate large forces and rapid bending motions [4], which are crucial for replicating the natural anguilliform swimming motion.

However, designing anguilliform-swimming soft fluidic robots presents significant challenges. The field lacks a widely accepted design methodology for determining optimal design parameters. The nonlinear material behavior of soft robots, combined with the complex fluid-structure interactions (FSI) involved in underwater swimming, make it difficult to rely solely on intuition or traditional design approaches. Multidisciplinary design optimization (MDO) offers a solution to this complexity by leveraging numerical models of multiple disciplines to simulate performance and systematically improve the design. There have been works in soft robotics which have successfully applied design optimization [5]; however these studies have typically been limited to single-discipline optimizations. For the control co-design optimization of a soft swimming robot, it is critical to capture both the fluid and structural effects to predict the performance of a design. On the other hand, MDO with fluid-structure interaction has been applied numerous times in fields such as aircraft design [6], [7]; however these applications typically focus on linearly elastic systems with significantly different behavior from soft robots.

This work investigates a method for performing multidisciplinary control co-design optimization with shape variables of anguilliform-swimming soft fluidic robots using physics-based models. The method combines a three-dimensional nonlinear finite element model to capture the robot's structural mechanics with an unsteady panel method to simulate the external fluid dynamics. To maintain consistency across disciplines, we employ a geometry-centric approach to geometry parametrization and modeling. This method is applied to optimize the design of an existing modular eel-inspired soft fluidic robot [8]. The design consists of three fluidic elastomer actuator modules which are arranged in series to produce anguilliform motion, a soft passive tail, and a rigid head (Figure 1). The computational model parameters are estimated and the model is validated using preexisting experimental data from the baseline design. Then, the models are used to perform an efficiency optimization of the soft robot. The optimized geometry of an actuator module is manufactured, and used to generate a new experimental data set. Using both the new and old data, the data assimilation is re-performed for the structural model and the actuator is re-optimized using the updated model parameters.

II. Related Work

Design optimization of soft robots has been explored using a variety of methods with considerable success in improving robotic performance through computational design. Chen and Wang provide a comprehensive review of the applications and strategies used in the optimization of soft robots [5].

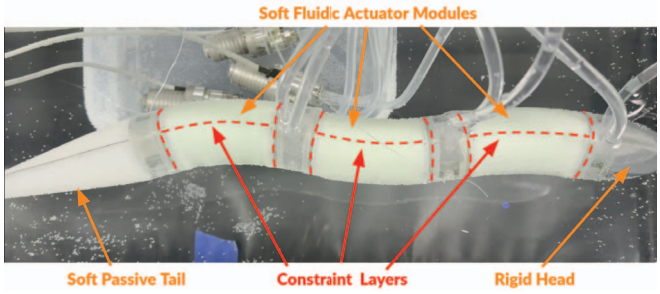

Fig. 1: The baseline design of the preexisting modular eel-inspired soft fluidic robot [8].

One common method for optimizing soft robots is through robot evolution approaches, which involve iterative improvement of design parameters using algorithms inspired by natural evolution. This technique was applied by Sims for optimizing rigid robots [9] and has since been extended to soft robotics in works such as Cheney et. al.'s multi-material walking robot [10], an optimization of a soft pneumatic robot [11], and an optimization of a flexible robotic fish fin [12]. Evolutionary algorithms and other gradient-free methods are well-regarded for their ability to explore the design space thoroughly, searching multiple local optima. However, these approaches generally require a large number of model evaluations to converge, with the computational cost scaling significantly as the number of design parameters grows. To maintain computational feasibility, optimizations using evolutionary approaches often limit the model fidelity or reduce the number of design variables.

Another prevalent optimization approach in soft robotics is topology optimization, which involves optimizing the material layout within a given geometric shape to achieve the best performance. Topology optimization has been used in the applications such as the design of cable-driven grippers [13], [14] , pneumatic actuators [15], [16], and a magnetically actuated soft actuator [17]. Topology optimization problems typically involve a large number of design variables, necessitating the use of gradient-based algorithms that rely on analytically computed derivatives. Gradient-based methods are favored due to their efficiency in exploring the design space, especially as the number of design variables increases, minimizing the number of model evaluations required to find an optimal solution. However, due to the large number of design variables and effort required to analytically derive derivatives, these studies often focus on static or linearly-elastic models and are typically limited to one or two disciplines.

In the context of optimizing anguilliform-swimming soft fluidic robots, the need for a multidisciplinary approach is critical. The performance of these robots are a function of the interactions between the structural and fluid dynamics. To perform optimization, the models must have sufficient fidelity to accurately map from design parameters to design performance. MDO approaches focus on solving design optimization problems with multidisciplinary models. While

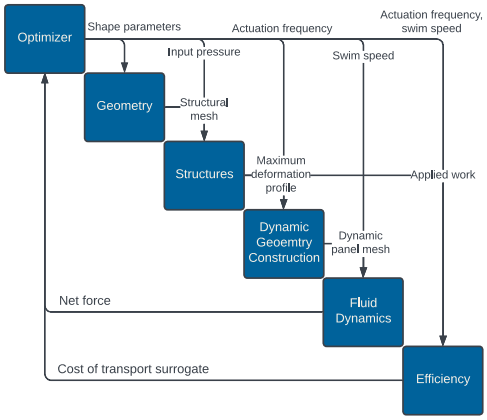

Fig. 2: Model Flowchart

MDO has most commonly been applied for aerospace applications, problems with FSI are especially common due to the importance of the effect in aircraft applications [6], [7]. In addition, physics-based models have been employed to perform 3D shape optimization [18], [7]. Similar to topology optimization, these approaches typically employ gradient-based optimizers with analytic derivative computation. As such, this study focuses on gradient-based optimization with medium-to-high-fidelity models to efficiently and effectively optimize the robot. On the other hand, typical MDO studies have focused on linearly elastic materials and steady fluid behavior. This study focuses on investigating a modeling approach for feasibility and accuracy for optimizing anguilliform-swimming soft fluidic robots.

III. Computational Modeling

A. Model Overview

The optimization method requires a computational model that accurately maps design parameters to design performance. The proposed approach identifies geometry, structures, and fluids as the necessary disciplines (Figure 2). The workflow is organized such that the design parameters first update the geometry model, which generates updated meshes for subsequent analysis. Using the pressure input and the structural mesh, the deformation of each actuator module is calculated to construct the dynamic, actuating geometry. The dynamic geometry is then used to evaluate the mesh and mesh velocities for external fluid dynamics. The external fluid dynamics model is used to compute the net force on the robot over an actuation period. The objective and constraints for the system optimization are defined based on mechanical work done on the structure, swimming speed, and net force on the robot.

To automate the derivation and computation of analytic derivatives, the models are implemented using the Computational System Design Language (CSDL) [19]. CSDL constructs a graph representation of the computational model, which is traversed backwards, computing the Jacobian-vector product for each operation to compute the total derivatives.

B. Geometry Modeling and parametrization

A geometry-centric modeling approach is employed, with a single high-fidelity representation serving as the basis for discipline-specific representations. For the central geometry, this study uses a B-spline volume function fitted to a CAD model of the baseline design. Meshes for each discipline model are stored using the coordinates of mesh nodes in the parametric space of the B-spline. Through shape optimization, as the control points of the central geometry are adjusted, the physical mesh coordinates are updated by reevaluating the geometry function at the mesh parametric coordinates, which are constant through the optimization.

A multilevel, deformation-based parametrization method is applied for the geometry parametrization. To reduce the number of design parameters and improve the robustness of the parametrization, free-form deformation (FFD) is used to directly parameterize the geometry. FFD stores the coordinates of the control points of the geometry in the parametric space of a simpler geometry function which is manipulated instead [20], [21]. In this work, a bounding B-spline volume is used as the FFD volume. The control points of the FFD volume are further parameterized using a sectional parametrization along a principal direction where the sections are made up of sets of the control points of the FFD volume. Four sections are defined along the width direction, where each section is able to stretch in the height and length directions. A nested optimization is formulated to meet high-level design variables, such as specified height and length, with the first-order optimality conditions serving as the residual for a Newton solver. To allow for low-level control of the shape of the cross-section of the robot, translations of the control points of the FFD volume on the outer sections in the width-direction are added as shape parameters. To maintain symmetry and reduce the dimensionality of the design problem, double symmetry is applied. By including the additional FFD sections surrounding the inner wall and only allowing the optimizer to manipulate the outer sections, the inner wall is held at a constraint thickness, which is a manufacturing constraint for the robot.

C. Structural Modeling and Dynamic Geometry Construction

The dynamic geometry modeling is split into two steps. In the first step, a single static finite element model is used to model the maximum deformation of one of the actuator modules. In the second step, the maximum deformation profile is used along with simplifying assumptions to construct the dynamic, actuating geometry.

The structural deformation is modeled using a three-dimensional finite element model with a nearly-incompressible Neo-Hookean material. The energy function is

$$\psi = \frac{\mu}{2}(\lambda_1^2 + \lambda_2^2 + \lambda_3^2 - 3) - \mu \ln(J) + \frac{\alpha}{2}(\ln(J))^2$$

with

$$\mu = \frac{E}{2(1+\nu)}, \quad \alpha = \frac{E\nu}{(1+\nu)(1-2\nu)}$$

where E is the Young's modulus, ν is the Poisson ratio, J is the determinant of the deformation gradient, and $\lambda_1^2+\lambda_2^2+\lambda_3^2$ is the trace of the Green deformation tensor. The third term in the energy function is a quadratic penalty on volume changes to enforce near-incompressibility. The weak form consists of the elastic energy's directional derivative minus the applied pressure load. The structural model is implemented using FEMO [22] and FEniCSx [23], with meshes generated by Gmsh [24] and projected into the geometry to find the nodal parametric coordinates. A continuous Galerkin function space with first-degree elements is used for the state function space. To account for the stiffer constraint layers in the center and edges of the actuator module, the elements in those regions are given a significantly higher Young's modulus and Poisson's ratio.

The dynamic geometry is derived from the static solution using simplifying assumptions for computational efficiency. The static finite element solution is used as the maximum deformation profile and is mirrored for actuation in the opposite direction. A linear interpolation between deformed, undeformed, and opposite states is used to model the movement of the actuator. Using the assumption that the chamber pressure and actuator deformation are sinusoidal in time, the interpolation weights are computed using a sine function. With the dynamic geometry of the actuator module, the deformation is propagated rigidly to adjacent modules. Additionally, the three modules deform identically, with phase offsets to create the traveling wave characteristic of anguilliform swimming.

D. External Fluid Dynamics Modeling

The external fluid dynamics are modeled using an unsteady panel method combined with a boundary layer model. By using a panel method, the model is able to capture the effects of thickness and three-dimensional perturbations in geometry. Using a vortex-based method rather than a computational fluid dynamics (CFD) method, the dynamics can be captured robustly with significantly lower computational cost.

E. Efficiency Modeling

System efficiency is evaluated using an approximate cost of transport metric, defined as the input power divided by swimming speed. Due to the absence of a dynamic motor and dynamic structural models, the input power is estimated with a surrogate metric, the applied mechanical work on the static structure divided by the actuation period, which has the same units and scales with the input power.

IV. Results

A. Data Assimilation and Model Validation

The structural finite element model was validated against existing experimental bending vs. pressure data [8] for the baseline actuator design. The Young's modulus and Poisson's ratio of the constraint layers were assumed to be $E_c = 3.7$ MPa and $\nu_c = 0.12$, respectively. To enforce near-incompressibility, the Poisson ratio of the soft material was

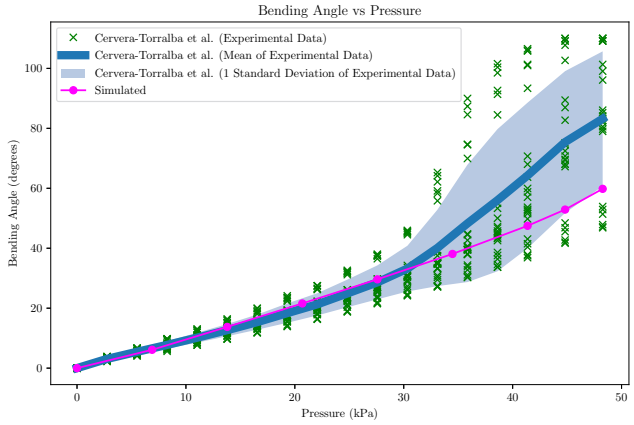

Fig. 3: The actuator bending angle, in degrees, is plotted against the chamber pressure, in kPa, for the simulated data (magenta circles) and the pre-existing experimental data (green) [8].

	High-level	Multilevel
Objective	Energy cost surrogate	Energy cost surrogate
Design Variables	Actuation freq.	Actuation freq.
	Max pump pressure	Max pump pressure
	Δ width (x1)	Δ width (x4)
	Height	Height
Constraint	Net force = 0	Net force = 0

TABLE I: Optimization Problem Formulations

set to $\nu_s = 0.499$. The experimental data enabled the estimation of the Young's modulus, found to be $E_s = 0.22$ MPa (Figure 3). With the given parameters, the root mean square error RMSE was 40.93 degrees. The numerical model exhibited a linear trend that closely matches actuators that had not undergone extensive cycling.

Validation and data assimilation for the fluid dynamics model was performed using existing experimental data [25]. The first step isolated skin friction drag by simulating the average net force for a range of swim speeds without actuation, and comparing the results to experimental measurements (Figure 4a). Matching the data required scaling the skin friction coefficient by a factor of 24, resulting in a RMSE of 0.027. The model was then validated with actuation, and to match experimental results, the inviscid term in the panel method was scaled by 1.8, yielding an RMSE of 0.019 N (Figure 4b).

B. Control Co-Design Optimization

Two different formulations of the control co-design problem were considered (Table I). Both aim to minimize the cost of transport with respect to control and shape parameters, subject to a constraint that the average net force equals zero. Additionally, a target swim speed of 0.66 body lengths per second was specified to ensure operational usability. One formulation uses a high-level parametrization with two control variables and two high-level shape variables, while the multi-level parametrization introduces low-level width variables to refine the robot's cross-sectional shape.

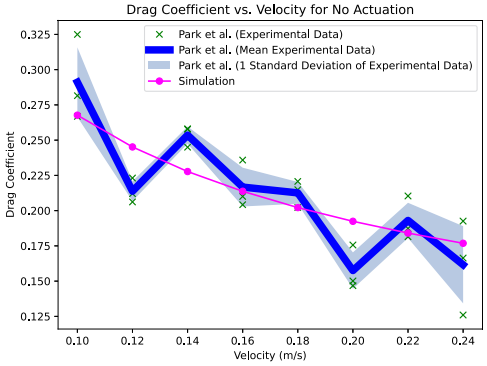

(a) The drag coefficient is plotted against the velocity, in m/s, for robot with no actuation.

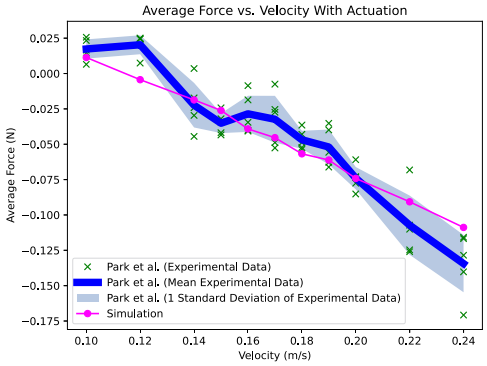

(b) The average force, in Newtons, is plotted against the velocity, in m/s for the actuating robot.

Fig. 4: Comparisons between simulation (magenta) and pre-existing experimental data [25] (green) to estimate the fluid dynamics model parameters

The optimization problem was solved using the PySLSQP optimizer [26], [27] within the modOpt environment [28]. In the high-level parametrization, the optimal solution featured a reduction in both width and height, while the multilevel parametrization resulted in more nuanced shape change with decreased width at the middle of the actuator with increased width near the top and bottom (Figure 5). The optimized design using the high-level parametrization resulted in a 55% lower simulated cost of transport with the prescribed 128% increase in swim speed compared to the baseline design with optimized control (Table II). The multilevel parametrization resulted in a 73% lower simulated cost of transport and the same prescribed 128% increase in swim speed compared to the baseline design.

C. Updated Data Assimilation and Optimization

The optimized module from the multilevel parametrization was fabricated, and its bending angle as a function of pressure was measured experimentally (Figure 6). The combination of the experimental data from the baseline and optimized designs were used to re-estimate the structural model parameters. The model parameters were found to be $E_s = 0.25$ MPa, $\nu_s = 0.42$, $E_c = 0.8$ GPa, and $\nu_c = 0.12$,

	Baseline	High-level	Multilevel	Updated
Energy cost surr.	2.408 J/m	0.914 J/m	0.649 J/m	1.316 J/m
Swim speed	0.13 m/s	0.297 m/s	0.297 m/s	0.297 m/s
Actuation freq.	0.679	0.708	0.716	0.730
Max pump pressure	28.3 kPa	26.7 kPa	24.7 kPa	36.6 kPa
Δ width 1	0	-31.9%	+28.7%	+19.7%
Δ width 2	0	N/A	-33.3%	-33.4%
Δ width 3	0	N/A	-39.8%	-39.4%
Δ width 4	0	N/A	-40%	-40%
Height	6.67 cm	8.33 cm	7.93 cm	5.59 cm

TABLE II: Optimization Results

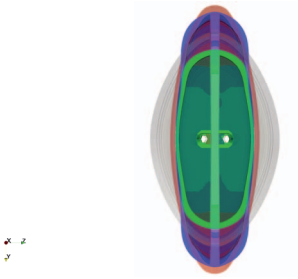

Fig. 5: The cross sections of the baseline (gray), high-level parametrization (red), multilevel parametrization (blue), and multilevel with updated model parameters (green) optimization results.

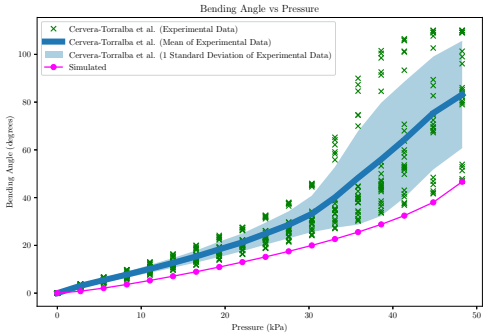

(a) Baseline design

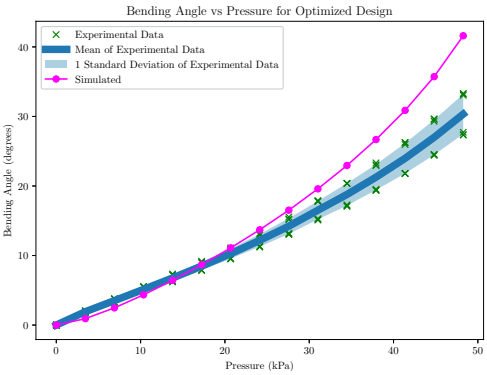

(b) Optimized design

Fig. 6: The actuator bending angle, in degrees, is plotted against the chamber pressure, in kPa, for the simulated data (magenta circles) and experimental data (green).

leading to an RMSE of 41.02 degrees for the baseline design and an RMSE of 16.05 degrees at the optimized design point.

With the new parameters, the system was optimized again using the multilevel shape parametrization (Table II). The approximate shape matches the initial optimization result, however the design variable values were noticeably different (Figure 5). The optimization showed a 45% decrease in the simulated energy cost and prescribed 128% increase in swim speed compared to the baseline design with optimal control with the updated model parameters.

V. Discussion

The structural model showed good agreement with experimental data for actuators that had undergone fewer actuation cycles. However, actuators with more cycles exhibited signs of geometric softening and strain stiffening at lower pressures, indicating changes in material properties over time. It is not clear whether the design optimization should target new or worn actuators. With the addition of another data set from the initially optimized actuator, there is a significant decrease in modeling error at the optimal design point. However, performing parameter estimation across four parameters proved to be a significant challenge and there still remains non-negligible error in the structural simulation at both design points.

The fluid dynamics model captured trends well, but required significant parameter tuning. The need for tuning the skin friction coefficient possibly results from the silicone-water interface producing significantly more drag than the aluminum-air interface that the method has typically been applied to. Additionally, tuning for the inviscid component may be due to the absence of a separation model in the current panel method implementation. Future efforts could incorporate a separation model to assess its impact on model accuracy. Despite these challenges, the fluid dynamics model showed good agreement with experimental results after data assimilation with only one scaling parameter for model section.

The optimization results showed substantial change in the robot design. Both high-level and multi-level optimizations lead to a reduced robot width, seemingly to decrease bending stiffness. In the multi-level parametrization, the optimizer has more control over the cross-sectional shape. With the increased control, the optimizer shapes the cross section to be more rectangular, seemingly to increase the torque-to-stiffness ratio, thus maximizing bending for a given pressure input. Finally, the optimizer seems to find the optimal balance between input pressure and height to generate the required thrust for the desired swimming speed.

After the additional parameter estimation step, the new optimization result showed a similar design concept to the initial optimization result, however the design parameter values and performance predictions changed significantly. This behavior suggests a potential approach of iteratively applying computational design optimization, manufacturing the optimized design, and re-estimating the model parameters using data from the newly acquired data in addition to the prior data.

VI. Conclusion

This study demonstrated the multidisciplinary control co-design for an anguilliform-swimming soft fluidic robot using gradient-based optimization with physics-based models. The models accurately captured performance trends, although data assimilation was necessary for accurate physics representation. The optimization approach proved to be computationally feasible, yielding significant performance improvements for both high-level and multilevel parametrizations. Additionally, the approach of iteratively manufacturing and optimizing the design is promising for converging to an optimal solution with little modeling error.

However, this study did not include manufacturing the entire optimized robot, and as such, the impact on metrics such as swimming speed, energy efficiency, or range remains experimentally unquantified. Future studies could consider manufacturing the full robot with the optimized geometry to directly measure the impact on system-level performance. Additionally, further research could increase modeling fidelity by incorporating structural dynamics or separation effects in the fluid model to decrease the reliance on experimental data for model accuracy. Moreover, additional disciplines, such as pump and battery modeling, could be included to optimize for energy consumption and range, providing a more comprehensive understanding of the robot's capabilities.

References

[1] S. Aracri, F. Giorgio-Serchi, G. Suaria, M. E. Sayed, M. P. Nemitz, S. Mahon, and A. A. Stokes, "Soft robots for ocean exploration and offshore operations: A perspective," *Soft Robotics*, vol. 8, no. 6, pp. 625–639, 2021, pMID: 33450174. [Online]. Available: https://doi.org/10.1089/soro.2020.0011

[2] R. K. Katzschmann, J. DelPreto, R. MacCurdy, and D. Rus, "Exploration of underwater life with an acoustically controlled soft robotic fish," *Science Robotics*, vol. 3, no. 16, p. eaar3449, 2018. [Online]. Available: https://www.science.org/doi/abs/10.1126/scirobotics.aar3449

[3] D. Q. Nguyen and V. A. Ho, "Anguilliform swimming performance of an eel-inspired soft robot," *Soft Robotics*, vol. 9, no. 3, pp. 425–439, 2022, pMID: 34134542. [Online]. Available: https://doi.org/10.1089/soro.2020.0093

[4] A. Pagoli, F. Chapelle, J.-A. Corrales-Ramon, Y. Mezouar, and Y. Lapusta, "Review of soft fluidic actuators: classification and materials modeling analysis," *Smart Materials and Structures*, vol. 31, no. 1, p. 013001, dec 2021. [Online]. Available: https://dx.doi.org/10.1088/1361-665X/ac383a

[5] F. Chen and M. Y. Wang, "Design optimization of soft robots: A review of the state of the art," *IEEE Robotics Automation Magazine*, vol. 27, no. 4, pp. 27–43, 2020.

[6] J. Jasa, J. Hwang, and J. Martins, "Open-source coupled aerostructural optimization using python," *Structural and Multidisciplinary Optimization*, vol. 57, 02 2018.

[7] G. Kenway, G. Kennedy, and J. R. R. A. Martins, *A CAD-Free Approach to High-Fidelity Aerostructural Optimization*. [Online]. Available: https://arc.aiaa.org/doi/abs/10.2514/6.2010-9231

[8] J. Cervera-Torralba, Y. Kang, E. M. Khan, I. Adibnazari, and M. T. Tolley, "Lost-core injection molding of fluidic elastomer actuators for the fabrication of a modular eel-inspired soft robot," in *2024 IEEE 7th International Conference on Soft Robotics (RoboSoft)*, 2024, pp. 971–976.

[9] K. Sims, "Evolving 3D Morphology and Behavior by Competition," *Artificial Life*, vol. 1, no. 4, pp. 353–372, 07 1994. [Online]. Available: https://doi.org/10.1162/artl.1994.1.4.353

[10] N. Cheney, R. MacCurdy, J. Clune, and H. Lipson, "Unshackling evolution: Evolving soft robots with multiple materials and a powerful generative encoding," 01 2013.

[11] D. M. Bodily, T. F. Allen, and M. D. Killpack, "Multi-objective design optimization of a soft, pneumatic robot," in *2017 IEEE International Conference on Robotics and Automation (ICRA)*, 2017, pp. 1864–1871.

[12] A. J. Clark, X. Tan, and P. K. McKinley, "Evolutionary multiobjective design of a flexible caudal fin for robotic fish," *Bioinspiration Biomimetics*, vol. 10, no. 6, p. 065006, nov 2015. [Online]. Available: https://dx.doi.org/10.1088/1748-3190/10/6/065006

[13] C.-H. Liu, T.-L. Chen, C.-H. Chiu, M.-C. Hsu, Y. Chen, T.-Y. Pai, W.-G. Peng, and Y.-P. Chiang, "Optimal design of a soft robotic gripper for grasping unknown objects," *Soft Robotics*, vol. 5, no. 4, pp. 452–465, 2018, pMID: 29741987. [Online]. Available: https://doi.org/10.1089/soro.2017.0121

[14] F. Chen, W. Xu, H. Zhang, Y. Wang, J. Cao, M. Y. Wang, H. Ren, J. Zhu, and Y. F. Zhang, "Topology optimized design, fabrication, and characterization of a soft cable-driven gripper," *IEEE Robotics and Automation Letters*, vol. 3, no. 3, pp. 2463–2470, 2018.

[15] H. Zhang, A. S. Kumar, F. Chen, J. Y. H. Fuh, and M. Y. Wang, "Topology optimized multimaterial soft fingers for applications on grippers, rehabilitation, and artificial hands," *IEEE/ASME Transactions on Mechatronics*, vol. 24, no. 1, pp. 120–131, 2019.

[16] Y. Chen, Z. Xia, and Q. Zhao, "Optimal design of soft pneumatic bending actuators subjected to design-dependent pressure loads," *IEEE/ASME Transactions on Mechatronics*, vol. 24, no. 6, pp. 2873–2884, 2019.

[17] J. Tian, X. Zhao, X. D. Gu, and S. Chen, "Designing ferromagnetic soft robots (ferrosoro) with level-set-based multiphysics topology optimization," in *2020 IEEE International Conference on Robotics and Automation (ICRA)*, 2020, pp. 10 067–10 074.

[18] C. Conlan-Smith, N. Ramos-García, O. Sigmund, and C. S. Andreasen, "Aerodynamic shape optimization of aircraft wings using panel methods," *AIAA Journal*, vol. 58, no. 9, pp. 3765–3776, 2020. [Online]. Available: https://doi.org/10.2514/1.J058979

[19] V. Gandarillas, A. J. Joshy, M. Sperry, A. Ivanov, and J. Hwang, "A graph-based methodology for constructing computational models that automates adjoint-based sensitivity analysis," *Structural and Multidisciplinary Optimization*, vol. 67, 05 2024.

[20] T. W. Sederberg and S. R. Parry, "Free-form deformation of solid geometric models," in *Proceedings of the 13th Annual Conference on Computer Graphics and Interactive Techniques*, ser. SIGGRAPH '86. New York, NY, USA: Association for Computing Machinery, 1986, p. 151–160. [Online]. Available: https://doi.org/10.1145/15922.15903

[21] J. Samareh, *Aerodynamic Shape Optimization Based on Free-Form Deformation*. [Online]. Available: https://arc.aiaa.org/doi/abs/10.2514/6.2004-4630

[22] R. Xiang, S. van Schie, L. Scotzniovsky, J. Yan, D. Kamensky, and J. Hwang, "Automating adjoint sensitivity analysis for multidisciplinary models involving partial differential equations," 07 2024.

[23] I. A. Baratta, J. P. Dean, J. S. Dokken, M. Habera, J. S. Hale, C. N. Richardson, M. E. Rognes, M. W. Scroggs, N. Sime, and G. N. Wells, "DOLFINx: the next generation FEniCS problem solving environment," preprint, 2023.

[24] C. Geuzaine and J.-F. Remacle, "Gmsh: A 3-d finite element mesh generator with built-in pre- and post-processing facilities," *International Journal for Numerical Methods in Engineering*, vol. 79, no. 11, pp. 1309–1331, 2009. [Online]. Available: https://onlinelibrary.wiley.com/doi/abs/10.1002/nme.2579

[25] M. Park, J. Cervera-Torralba, I. Adibnazari, and M. T. Tolley, "Analysis on kinematics and propulsion of a self-sensing multi-dof undulating robotic fish," Under Review.

[26] A. J. Joshy and J. T. Hwang, "Pyslsqp: A transparent python package for the slsqp optimization algorithm modernized with utilities for visualization and post-processing," *arXiv preprint arXiv:2408.13420*, 2024.

[27] D. Kraft, "A software package for sequential quadratic programming," *Forschungsbericht- Deutsche Forschungs- und Versuchsanstalt fur Luft- und Raumfahrt*, 1988.

[28] A. J. Joshy and J. T. Hwang, "modopt: A modular development environment and library for optimization algorithms," *arXiv preprint arXiv:2410.12942*, 2024.